Quantum path-integral II

Lester Ingber
Lester Ingber Research, Ashland, Oregon 97520
Email: ingber@alumni.caltech.edu [https://www.ingber.com]

Abstract

Background

A path-integral algorithm, PATHINT used previously for several systems, has been generalized from 1 dimension to N dimensions, and from classical to quantum systems into qPATHINT. Previous publications applied qPATHINT to two systems developed by the author, in neocortical interactions and financial options. Also, previous publications using classical PATHINT have developed a statistical mechanics of neocortical interactions (SMNI) that has been fitted to EEG data under attentional experimental paradigms. Classical PATHINT also has been published demonstrating development of Eurodollar options in industrial applications.

Objective

A study is required to see if the qPATHINT algorithm can scale sufficiently to further develop real-world calculations in these two systems, requiring interactions between classical and quantum scales. A new algorithm is needed to develop interactions between classical and quantum scales.

Method

Both systems are developed using mathematical-physics methods of path integrals in quantum spaces. Supercomputer pilot studies using XSEDE.org resources tested various dimensions for their scaling limits. For the financial options study, all traded Greeks are calculated for Eurodollar options in quantum-money spaces. For the neuroscience study, tripartite neuron-astrocyte-neuron Ca-ion waves are propagated for 100's of msec. For the neuroscience system, the quantum path-integral is used to derive a closed-form analytic solution at arbitrary time, in the absence of shocks, that is used to calculate classical-physics interactions among scales.

Results

The mathematical-physics and computer parts of the study are successful for both systems. A 3-dimensional path-integral propagation of qPATHINT for both systems is within normal computational bounds on supercomputers. The neuroscience quantum path-integral also has a closed solution at arbitrary time that tests the multiple-scale model including the quantum scale.

Conclusion

Each of the two systems considered contribute insight into applications of qPATHINT to the other system, leading to new algorithms presenting time-dependent propagation of interacting

quantum and classical scales. This can be achieved by propagating qPATHINT and PATHINT in synchronous time for the interacting systems, which is a future set of studies.

Key words: path integral, quantum mechanics, blockchains, parallel code, financial options

1 Introduction

There is a long list of governments and companies developing hardware and software for quantum computing. A recent list includes:

D-WAVE (Canada)
DeepMind (Canada)
Facebook
Google
IBM
Intel
Microsoft
National Laboratory for Quantum Information Sciences (China)
Nippon Telegraph and Telephone
NOKIA Bell Labs
NSA
Post-Quantum
Rigetti
Russian Quantum Center
Toshiba
Quantum Circuits
Quantum Technologies (European Union)

Since error correction is a vital consideration for quantum computers, this is a major task being addressed.

It is inevitable that these developments in quantum hardware and software will spin off into all levels of schools and post-education, and eventually products and services based on quantum processes will be offered for general consumption. Then, it is a small step forward to appreciate that some new quantum products will require calculations using quantum variables *per se*, beyond quantum computation.

An N-dimensional code, qPATHINT, has been developed to calculate the propagation of quantum variables in the presence of shocks, since many real systems propagate in the presence of shocks, defined here as sudden changes of state dependent on time. qPATHINT is based on a classical-physics code, PATHINT, which has demonstrated its usefulness in several systems across several disciplines, including neuroscience and financial derivatives. This paper deals specifically with two such systems, Statistical Mechanics of Neocortical Interactions (SMFM) and Statistical Mechanics of Financal Markets (SMFM).

Section 2 defines the PATHINT algorithm and its utility.

Section 3 describes a different algorithm, ASA, used for optimization of many systems – fitting models to real data, e.g., those considered here for further development by qPATHINT, as well as fits to EEG data reported here.

Section 4 gives a brief summary of the neuroscience project further developed here for inclusion of quantum scales.

Section 5 gives a brief summary of the finance project further developed here for inclusion of quantum scales.

Section 6 gives details of the qPATHINT code, and lessons learned from recent pilot studies projects including quantum scales in the neuroscience and finance projects.

Section 7 describes some applications already evident from these two quantum-scale projects.

Section 8 is the Conclusion.

2 PATHINT

2.1 Path Integral in Stratonovich (Midpoint) Representation

The path integral in the Feynman (midpoint) representation is most suitable for examining discretization issues in time-dependent nonlinear systems (Langouche et al., 1979, 1982; Schulman, 1981). (N.b. $g^\dagger$ in DM implies a prepoint evaluation.) Unless explicitly otherwise, the Einstein summation convention is used, wherein repeated indices signify summation; bars $|\dots|$ imply no summation.

$$P[M_t|M_{t_0}]dM(t) = \int \dots \int DM \exp\left(-\min \int_{t_0}^{t} dt' L\right) \delta\big(M(t_0) = M_0\big)\delta\big(M(t) = M_t\big)$$

$$DM = \lim_{u\to\infty} \prod_{\rho=1}^{u+1} g^{\dagger 1/2} \prod_G (2\pi\theta)^{-1/2} dM_\rho^G$$

$$L(\dot{M}^G, M^G, t) = \frac{1}{2}(\dot{M}^G - h^G)g_{GG'}(\dot{M}^{G'} - h^{G'}) + \frac{1}{2}h^G_{;G} + R/6 - V$$

$$\dot{M}^G(t) \to M^G_{\rho+1} - M^G_\rho, M^G(t) \to \frac{1}{2}(M^G_{\rho+1} + M^G_\rho), [\dots]_{,G} = \frac{\partial[\dots]}{\partial M^G}$$

$$h^G = g^G - \frac{1}{2}g^{-1/2}(g^{1/2}g^{GG'})_{,G'}, h^G_{;G} = h^G_{,G} + \Gamma^F_{GF}h^G = g^{-1/2}(g^{1/2}h^G)_{,G}$$

$$g_{GG'} = (g^{GG'})^{-1}, g = \det(g_{GG'})$$

$$\Gamma^F_{JK} \equiv g^{LF}[JK, L] = g^{LF}(g_{JL,K} + g_{KL,J} - g_{JK,L})$$

$$R = g^{JL}R_{JL} = g^{JL}g^{JK}R_{FJKL}$$

$$R_{FJKL} = \frac{1}{2}(g_{FK,JL} - g_{JK,FL} - g_{FL,JK} + g_{JL,FK}) + g_{MN}(\Gamma^M_{FK}\Gamma^N_{JL} - \Gamma^M_{FL}\Gamma^N_{JK}) \qquad (1)$$

2.2 Path Integral in Ito (Prepoint) Representation

For conditional probability distributions or for wave functions, in the Ito (prepoint) representation:

$$P[M_t|M_{t_0}]dM(t) = \int \ldots \int DM \exp\big(-\min \int_{t_0}^{t} dt' L\big)\delta\big(M(t_0) = M_0\big)\delta\big(M(t) = M_t\big)$$

$$DM = \lim_{u\to\infty} \prod_{\rho=1}^{u+1} g^{1/2} \prod_{G} (2\pi\Delta t)^{-1/2} dM_\rho^G$$

$$L(\dot{M}^G, M^G, t) = \frac{1}{2}(\dot{M}^G - g^G)g_{GG'}(\dot{M}^{G'} - g^{G'}) + R/6$$

$$\dot{M}^G(t) \to M_{\rho+1}^G - M_\rho^G, M^G(t) \to M_\rho^G$$

$$g_{GG'} = (g^{GG'})^{-1}, g = \det(g_{GG'}) \tag{2}$$

Here the diagonal diffusion terms are $g^{|GG|}$ and the drift terms are g^G. If the diffusions terms are not constant, then there are additional terms in the drift, and in a Riemannian-curvature potential $R/6$ for dimension > 1 in the midpoint Stratonovich/Feynman discretization.

2.3 Path-Integral Riemannian Geometry

The midpoint derivation explicitly derives a Riemannian geometry induced by these statistics, with a metric defined by the inverse of the covariance matrix

$$g_{GG'} = (g^{GG'})^{-1} \tag{3}$$

and where R is the Riemannian curvature

$$R = g^{JL}R_{JL} = g^{JL}g^{JK}R_{FJKL} \tag{4}$$

An Ito prepoint discretization for the same probability distribution P gives a much simpler algebraic form,

$$M(\bar{t}_s) = M(t_s)$$

$$L = \frac{1}{2}(dM^G/dt - g^G)g_{GG'}(dM^{G'}/dt - g^{G'}) - V \tag{5}$$

but the Lagrangian L so specified does not satisfy a variational principle useful for moderate to large noise; its associated variational principle only provides information useful in the weak-noise limit. Numerically, this often means that finer meshes are required for calculations for the prepoint representation.

2.4 Three Approaches Are Mathematically Equivalent

Three basic different approaches are mathematically equivalent:

(a) Fokker-Planck/Chapman-Kolmogorov partial-differential equations
(b) Langevin coupled stochastic-differential equations
(c) Lagrangian or Hamiltonian path-integrals

The path-integral approach is particularly useful to precisely define intuitive physical variables from the Lagrangian L in terms of its underlying variables M^G:

$$\text{Momentum}: \ \Pi^G = \frac{\partial L}{\partial(\partial M^G/\partial t)}$$

$$\text{Mass}: \ g_{GG'} = \frac{\partial L}{\partial(\partial M^G/\partial t)\partial(\partial M^{G'}/\partial t)}$$

$$\text{Force}: \ \frac{\partial L}{\partial M^G}$$

$$F = ma: \ \delta L = 0 = \frac{\partial L}{\partial M^G} - \frac{\partial}{\partial t}\frac{\partial L}{\partial(\partial M^G/\partial t)} \tag{6}$$

Differentiation especially of noisy systems often introduces more noise. Integration is inherently a smoothing process, and so the path-integral often gives superior numerical performance.

2.5 Stochastic Differential Equation (SDE)

The Stratonovich (midpoint discretized) Langevin equations can be analyzed in terms of the Wiener process dW^i, which can be rewritten in terms of Gaussian noise $\eta^i = dW^i/dt$ if care is taken in the limit.

$$dM^G = f^G\big(t, M(t)\big)dt + \hat{g}_i^G\big(t, M(t)\big)dW^i$$

$$\dot{M}^G(t) = f^G\big(t, M(t)\big) + \hat{g}_i^G\big(t, M(t)\big)\eta^i(t)$$

$$dW^i \to \eta^i dt$$

$$M = \{M^G; G = 1, \ldots, \Lambda\}$$

$$\eta = \{\eta^i; i = 1, \ldots, N\}$$

$$\dot{M}^G = dM^G/dt$$

$$< \eta^j(t) >_\eta = 0, < \eta^j(t), \eta^{j'}(t') >_\eta = \delta^{jj'}\delta(t - t') \tag{7}$$

η^i represents Gaussian white noise.

2.6 Partial Differential Equation (PDE)

The Fokker-Planck, or Chapman-Kolmogorov, partial differential equation is:

$$P_{,t} = \frac{1}{2}(g^{GG'}P)_{,GG'} - (g^{G}P)_{,G} + VP$$

$$P =< P_\eta >_\eta$$

$$g^G = f^G + \frac{1}{2}\hat{g}_i^{G'}\hat{g}_{i,G'}^{G}$$

$$g^{GG'} = \hat{g}_i^G \hat{g}_i^{G'}$$

$$(\ldots)_{,G} = \partial(\ldots)/\partial M^G \tag{8}$$

g^G replaces f^G in the SDE if the Ito (prepoint discretized) calculus is used to define that equation. If some boundary conditions are added as Lagrange multipliers, these enter as a "potential" V, creating a Schrodinger-type equation.

2.7 Applications

Path integrals and PATHINT have been applied across several disciplines, including combat simulations (Ingber et al., 1991), neuroscience (Ingber, 1994, 2017a; Ingber and Nunez, 1995, 2010), finance (Ingber, 2000, 2016a, 2017a,b,c; Ingber et al., 2001; Ingber and Wilson, 2000), and other nonlinear systems (Ingber, 1995a, 1998a; Ingber et al., 1996).

3 Adaptive Simulated Annealing (ASA)

3.1 Importance Sampling

Nonlinear systems present complex spaces, often requiring methods of importance-sampling to scan or to fit parameters. Methods of simulated annealing (SA) are often used. Proper annealing (not "quenching") possesses a proof of finding the deepest minimum in searches.

The ASA code is open-source software, and can be downloaded and used without any cost or registration at https://www.ingber.com/#ASA (Ingber, 1993a, 2012a).

This algorithm fits empirical data to a theoretical cost function over a D-dimensional parameter space, adapting for varying sensitivities of parameters during the fit.

Heuristic arguments have been developed to demonstrate that this ASA algorithm is faster than the fast Cauchy annealing, $T_i = T_0/k$, and much faster than Boltzmann annealing, $T_i = T_0/\ln k$ (Ingber, 1989).

3.2 Outline of ASA Algorithm

For parameters

$$\alpha_k^i \in [A_i, B_i]$$

sampling with the random variable x^i

$$x^i \in [-1, 1]$$

$$\alpha_{k+1}^i = \alpha_k^i + x^i(B_i - A_i)$$

the default generating function is

$$g_T(x) = \prod_{i=1}^{D} \frac{1}{2\,\ln(1 + 1/T_i)(|x^i| + T_i)} \equiv \prod_{i=1}^{D} g_T^i(x^i)$$

in terms of parameter "temperatures"

$$T_i = T_{i0} \exp(-c_i k^{1/D}) \tag{9}$$

It has proven fruitful to use the same type of annealing schedule for the acceptance function h as used for the generating function g, but with the number of acceptance points, instead of the number of generated points, used to determine the k for the acceptance temperature.

All default functions in ASA can be overridden with user-defined functions.

3.3 Hills and Valleys

It helps to visualize the problems presented by such complex systems as a geographical terrain. For example, consider a mountain range, with two "parameters," e.g., along the North-South and East-West directions. We wish to find the lowest valley in this terrain. SA approaches this problem similar to using a bouncing ball that can bounce over mountains from valley to valley.

We start at a high "temperature," where the temperature is an SA parameter that mimics the effect of a fast moving particle in a hot object like a hot molten metal, thereby permitting the ball to make very high bounces and being able to bounce over any mountain to access any valley, given enough bounces. As the temperature is made relatively colder, the ball cannot bounce so high, and it also can settle to become trapped in relatively smaller ranges of valleys. This process is often implemented in qubit-hardware in quantum computers.

We imagine that our mountain range is aptly described by a "cost function." We define probability distributions of the two directional parameters, called generating distributions since they generate possible valleys or states we are to explore.

We define another distribution, called the acceptance distribution, which depends on the difference of cost functions of the present generated valley we are to explore and the last saved lowest valley. The acceptance distribution decides probabilistically whether to stay in a new lower valley or to bounce out of it. All the generating and acceptance distributions depend on temperatures.

3.4 Applications

ASA and its predecessor Very Fast Simulated Reannealing (VFSR) have been used to fit data by many researchers, including the author in a range of disciplines:

chaotic systems (Ingber et al., 1996)
combat simulations (Ingber, 1993b, 1998a)
financial systems: bonds, equities, futures, options (Ingber, 1990, 1996a, 2000, 2005; Ingber et al., 2001; Ingber and Mondescu, 2003)
neuroscience (Ingber, 1991, 1992, 1996b, 1997a, 1998b, 2006a, 2009a,b, 2012b,c, 2013, 2015; Ingber and Nunez, 1995, 2010; Ingber et al., 2014, 1996; Nunez et al., 2013)

optimization *per se* (Atiya et al., 2003; Ingber, 1989, 1993c, 1996c, 2012a; Ingber and Rosen, 1992)

4 Statistical Mechanics of Neocortical Interactions (SMNI)

The project Statistical Mechanics of Neocortical Interactions (SMNI) has been developed in over 30+ papers since 1981, scaling aggregate synaptic interactions to describe neuronal firings, then scaling minicolumnar-macrocolumnar columns of neurons to mesocolumnar dynamics, and then scaling columns of neuronal firings to regional (sensory) macroscopic sites identified in electroencephalographic (EEG) studies (Ingber, 1981, 1982, 1983, 1984, 1985a, 1994).

The measure of the success of SMNI has been to discover agreement/fits with experimental data from various modeled aspects of neocortical interactions, e.g., properties of short-term memory (STM) (Ingber, 2012b), including its capacity (auditory 7 ± 2 and visual 4 ± 2) (Ericsson and Chase, 1982; Zhang and Simon, 1985), duration, stability , primacy versus recency rule, as well other phenomenon, e.g., Hick's law (Hick, 1952; Ingber, 1999; Jensen, 1987), nearest-neighbor minicolumnar interactions within macrocolumns calculating rotation of images, etc (Ingber, 1982, 1983, 1984, 1985a, 1994). SMNI was also scaled to include mesocolumns across neocortical regions to fit EEG data (Ingber, 1997a,b, 2012b).

4.1 Model of Models (MOM)

Deep Learning (DL) has invigorated AI approaches to parsing data in complex systems, often to develop control processes of these systems. A couple of decades ago, Neural Net AI approaches fell out of favor when concerns were apparent that such approaches offered little guidance to explain the "why" or "how" such algorithms worked to process data, e.g., contexts which were deemed important to deal with future events and outliers, etc.

The success of DL has overshadowed these concerns. However, that should not diminish their importance, especially if such systems are placed in positions to affect lives and human concerns; humans are ultimately responsible for structures they build.

An approach to dealing with these concerns can be called Model of Models (MOM). An argument in favor of MOM is that humans over thousands of years have developed models of reality across many disciplines, e.g., ranging over Physics, Biology, Mathematics, Economics, etc.

A good use of DL might be to process data for a given system in terms of a collection of models, then again use DL to process the models over the same data to determine a superior model of models (MOM). Eventually, large DL (quantum) machines could possess a database of hundreds or thousands of models across many disciplines, and directly find the best (hybrid) MOM for a given system.

In particular, SMNI offers a reasonable model upon which to further develop MOM, wherein multiple scales of observed interactions are developed. This is depicted in Fig. 1.

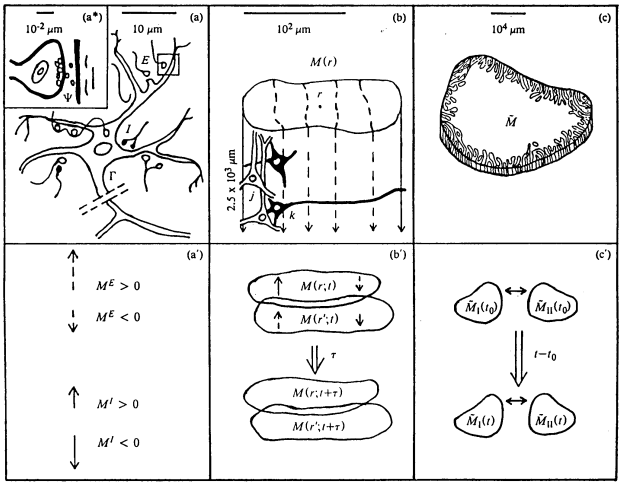

Figure 1 illustrates three SMNI biophysical scales (Ingber, 1982, 1983): (a)-(a*)-(a') microscopic neurons; (b)-(b') mesocolumnar domains; (c)-(c') macroscopic regions.
(a*): synaptic inter-neuronal interactions, averaged over by mesocolumns, are phenomenologically described by the mean and variance of a distribution Ψ (a): intraneuronal transmissions phenomenologically described by the mean and variance of Γ (a'): collective mesocolumnar-averaged inhibitory (I) and excitatory (E) neuronal firings M
(b): vertical organization of minicolumns together with their horizontal stratification, yielding a physiological entity, the mesocolumn (b'): overlap of interacting mesocolumns at locations r and r' from times t and $t+\tau$, τ on the order of 10 msec
(c): macroscopic regions of neocortex arising from many mesocolumnar domains (c'): regions coupled by long-ranged interactions

4.1.1 Ideas by Statistical Mechanics

A project sympathetic to this MOM context was proposed as Ideas by Statistical Mechanics (ISM) (Ingber, 2006b, 2007, 2008). using Adaptive Simulated Annealing (ASA) (Ingber, 1989, 1993a, 2012a) to fit parameters of a generic nonlinear multivariate colored-noise Gaussian-Markovian short-time conditional probability distribution to data, useful for many systems.

Models developed using ASA have been applied in many contexts across many systems (Ingber, 1993c), including applications to neural networks (Atiya et al., 2003).

Many of these ASA applications have used Ordinal representations of features, to permit parameterization of their inclusion into models, quite similar in spirit to DL.

ASA can be used again in the expanded context of MOM. This is suggested as a first step in a new discipline to which MOM is to be applied, to help develop a range of parameters useful for DL, as DL by itself may get stuck in non-ideal local minima of the importance-sampled space. Then, after a reasonable range of models is found, DL can take over to permit much more efficient and accurate development of MOM for a given discipline/system.

4.2 SMNI Development

4.2.1 Synaptic Interactions

The derivation of chemical inter-neuronal and electrical intra-neuronal interactions yields a short-time probability distribution of a given neuron firing due to its just-previous interactions with other neurons (Ingber, 1982, 1983). Within $\tau_j$neuron j fires ($\sigma_j = +1$) or does not fire ($\sigma_j = -1$), given its previous interactions with k neurons, is

$$p_{\sigma_j} = \Gamma\Psi = \frac{\exp(-\sigma_j F_j)}{\exp(F_j) + \exp(-F_j)}$$

$$F_j = \frac{V_j - \sum_k a^*_{jk} v_{jk}}{\left(\pi \sum_{k'} a^*_{jk'} (v^2_{jk'} + \phi^2_{jk'})\right)^{1/2}}$$

$$a_{jk} = \frac{1}{2} A_{|jk|}(\sigma_k + 1) + B_{jk} \tag{10}$$

Γ represents the "intra-neuronal" probability distribution, e.g., of a contribution to polarization achieved at an axon given activity at a synapse, taking into account averaging over different neurons, geometries, etc. Ψ represents the "inter-neuronal" probability distribution, e.g., of thousands of quanta of neurotransmitters released at one neuron's postsynaptic site effecting a (hyper-)polarization at another neuron's presynaptic site, taking into account interactions with neuromodulators, etc. This development is true for Γ Poisson, and for Ψ Poisson or Gaussian.

V_j is the depolarization threshold in the somatic-axonal region, v_{jk} is the induced synaptic polarization of E or I type at the axon, and ϕ_{jk} is its variance. The efficacy a_{jk}, related to the inverse conductivity across synaptic gaps, is composed of a contribution A_{jk} from the connectivity between neurons which is activated if the impinging k-neuron fires, and a contribution B_{jk} from spontaneous background noise.

4.2.2 Neuronal Interactions

The microscopic synaptic scale is aggregated up to the mesoscopic scale, using

$$P = \prod_G P^G[M^G(r; t+\tau) | M^{\bar{G}}(r'; t)]$$

$$= \sum_{\sigma_j} \delta \left(\sum_{jE} \sigma_j - M^E(r; t+\tau) \right) \delta \left(\sum_{jI} \sigma_j - M^I(r; t+\tau) \right) \prod_j^N p_{\sigma_j} \tag{11}$$

where M represents a mesoscopic scale of columns of N neurons, with subsets E and I, represented by p_{q_i}, constrained by the "delta"-functions δ, representing an aggregate of many neurons in a

column. G is used to represent excitatory (E) and inhibitory (I) contributions. $\bar{G}$ designates contributions from both E and I.

In the limit of many neurons per minicolumn, a path integral is derived with mesoscopic Lagrangian L, defining the short-time probability distribution of firings in a minicolumn, composed of given its just previous interactions with all other neurons in its macrocolumnar surround.

4.2.3 Columnar Interactions

The SMNI Lagrangian L in the prepoint (Ito) representation is

$$L = \sum_{G,G'} (2N)^{-1} (\dot{M}^G - g^G) g_{GG'} (\dot{M}^{G'} - g^{G'}) / (2N\tau) - V'$$

$$g^G = -\tau^{-1} (M^G + N^G \tanh F^G)$$

$$g^{GG'} = (g_{GG'})^{-1} = \delta^{G'}_G \tau^{-1} N^G \mathrm{sech}^2 F^G$$

$$g = \det(g_{GG'}) \tag{12}$$

The threshold factor F^G is derived as

$$F^G = \sum_{G'} \frac{\nu^G + \nu^{\ddagger E'}}{\left((\pi/2)[(v^G_{G'})^2 + (\phi^G_{G'})^2](\delta^G + \delta^{\ddagger E'})\right)^{1/2}}$$

$$\nu^G = V^G - a^G_{G'} v^G_{G'} N^{G'} - \frac{1}{2} A^G_{G'} v^G_{G'} M^{G'}, \nu^{\ddagger E'} = -a^{\ddagger E}_{E'} v^E_{E'} N^{\ddagger E'} - \frac{1}{2} A^{\ddagger E}_{E'} v^E_{E'} M^{\ddagger E'}$$

$$\delta^G = a^G_{G'} N^{G'} + \frac{1}{2} A^G_{G'} M^{G'}, \delta^{\ddagger E'} = a^{\ddagger E}_{E'} N^{\ddagger E'} + \frac{1}{2} A^{\ddagger E}_{E'} M^{\ddagger E'}$$

$$a^G_{G'} = \frac{1}{2} A^G_{G'} + B^G_{G'}, a^{\ddagger E}_{E'} = \frac{1}{2} A^{\ddagger E}_{E'} + B^{\ddagger E}_{E'} \tag{13}$$

where $A^G_{G'}$ is the columnar-averaged direct synaptic efficacy, $B^G_{G'}$ is the columnar-averaged background-noise contribution to synaptic efficacy. $A^G_{G'}$ and $B^G_{G'}$ have been scaled by $N^*/N \approx 10^3$ keeping F^G invariant. The "‡" parameters arise from regional interactions across many macrocolumns.

4.2.4 SMNI Parameters From Experiments

All values of parameters and their bounds are taken from experimental data, not arbitrarily fit to specific phenomena.

$N^G = \{N^E = 160, N^I = 60\}$ was chosen for visual neocortex, $\{N^E = 80, N^I = 30\}$ was chosen for all other neocortical regions, $M^{G'}$ and $N^{G'}$ in F^G are afferent macrocolumnar firings scaled to efferent minicolumnar firings by $N/N^* \approx 10^{-3}$, and N^* is the number of neurons in a macrocolumn, about 10^5. V' includes nearest-neighbor mesocolumnar interactions. τ is usually considered to be on the order of 5-10 ms.

Other values also are consistent with experimental data, e.g., $V^G = 10$ mV, $v^G_{G'} = 0.1$ mV, $\phi^G_{G'} = 0.03^{1/2}$ mV.

Nearest-neighbor interactions among columns give dispersion relations that were used to calculate speeds of visual rotation.

The variational principal applied to the SMNI Lagrangian also has been used to derive the wave equation cited by EEG theorists, permitting fits of SMNI to EEG data (Ingber, 1995b).

Note the audit trail of synaptic parameters from synaptic statistics within a neuron to the statistically averaged regional SMNI Lagrangian.

4.3 Previous Applications

4.3.1 Verification of basic SMNI Hypothesis

Only circa 2012 has the core SMNI hypothesis since circa 1980 (Ingber, 1981, 1982, 1983), that highly synchronous patterns of neuronal firings in fact process high-level information, been verified experimentally (Asher, 2012; Salazar et al., 2012).

4.3.2 SMNI Calculations of Short-Term Memory (STM)

SMNI calculations agree with observations (Ingber, 1982, 1983, 1984, 1985a, 1994, 1995c, 1997a, 1999, 2011, 2012b,c, 2015, 2016b, 2017a,b; Ingber et al., 2014; Nunez et al., 2013): This list includes:

capacity (auditory 7 ± 2 and visual 4 ± 2) (Ingber, 1984)
duration (Ingber, 1985a)
stability (Ingber, 1985a)
primacy versus recency rule (Ingber, 1985a,b)
Hick's law (reaction time and g factor) (Ingber, 1999)
nearest-neighbor minicolumnar interactions => rotation of images (Ingber, 1982, 1983)
derivation of basis for EEG (Ingber, 1985c, 1995b)

4.3.3 Three Basic SMNI Models

Three basic models were developed with slight adjustments of the parameters, changing the firing component of the columnar-averaged efficacies $A^G_{G'}$ within experimental ranges, which modify F^G threshold factors to yield in the conditional probability:

(a) case EC, dominant excitation subsequent firings
(b) case IC, inhibitory subsequent firings
(c) case BC, balanced between EC and IC

Consistent with experimental evidence of shifts in background synaptic activity under conditions of selective attention, a Centering Mechanism (CM) on case BC yields case BC$'$ wherein the numerator of F^G only has terms proportional to $M^{E'}$, $M^{I'}$ and $M^{\ddagger E'}$, i.e., zeroing other constant terms by resetting the background parameters $B^G_{G'}$, still within experimental ranges. This has the net effect of bringing in a maximum number of minima into the physical firing M^G-space. The minima of the numerator then defines a major parabolic trough,

$$A^E_E M^E - A^E_I M^I = 0 \tag{14}$$

about which other SMNI nonlinearities bring in multiple minima calculated to be consistent with STM phenomena.

In recent projects a Dynamic CM (DCM) model is used as well, wherein the $B^G_{G'}$ are reset every few epochs of τ. Such changes in background synaptic activity are seen during attentional tasks (Briggs et al., 2013).

4.3.4 PATHINT STM

The evolution of a Balanced Centered model (BC) after 500 foldings of $\Delta t = 0.01$, or 5 unit of relaxation time τ exhibits the existence of ten well developed peaks or possible trappings of firing patterns.

This describes the "7 ± 2" rule, as calculated by SMNI PATHINT in Fig. 2.

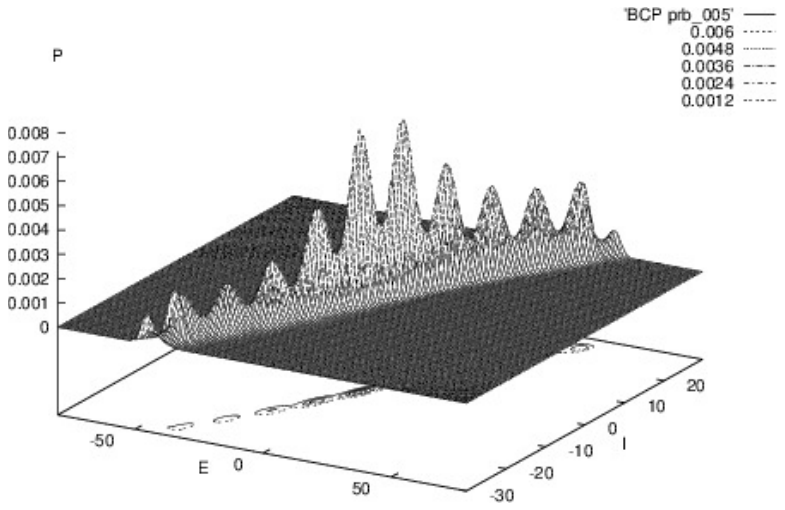

Figure 2 illustrates SMNI STM Model BC at the evolution at 5τ (Ingber and Nunez, 1995).

4.3.5 PATHINT STM Visual

The evolution of a Balanced Centered Visual model (BCV) after 1000 foldings of $\Delta t = 0.01$, or 10 unit of relaxation time τ exhibits the existence of four well developed peaks or possible trappings of firing patterns. Other peaks at lower scales are clearly present, numbering on the same order as in the BC' model, as the strength in the original peaks dissipates throughout firing space, but these are much smaller and therefore much less probable to be accessed.

This describes the "4 ± 2" rule for visual STM, as calculated by SMNI PATHINT in Fig. 3.

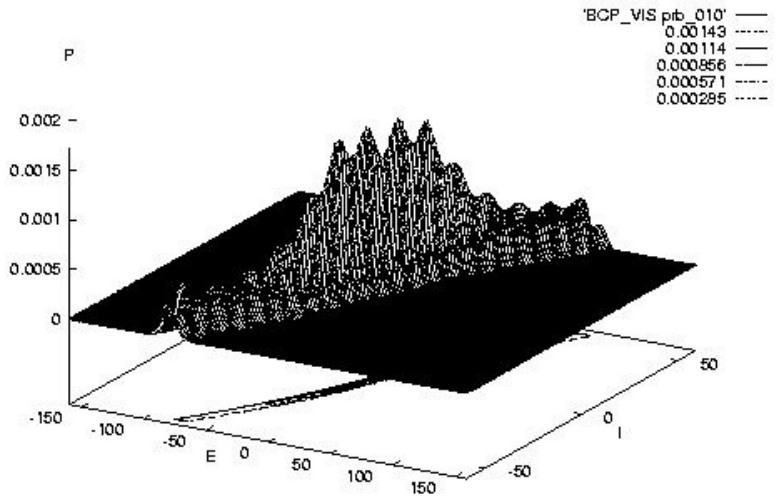

Figure 3 illustrates SMNI STM Model BCV at the evolution at 10τ (Ingber and Nunez, 1995).

4.4 Tripartite Synaptic Interactions

The human brain contains over 10^{11} cells, about half of which are neurons, and the other half are glial cells. Astrocytes comprise a good fraction of glial cells, possibly the majority. Many papers examine the influence of astrocytes on synaptic processes (Agulhon et al., 2008; Araque and Navarrete, 2010; Banaclocha et al., 2010; Bellinger, 2005; Innocenti et al., 2000; Pereira and Furlan, 2009; Reyes and Parpura, 2009; Scemes and Giaume, 2006; Volterra et al., 2014).

http://www.astrocyte.info claims:

> They are the most numerous cells in the human brain. [...] Astrocytes outnumber neurons 50:1 and are very active in the central nervous system, unlike previous ideology of astrocytes being "filler" cells.

Glutamate release from astrocytes through a Ca^{2+}-dependent mechanism can activate receptors located at the presynaptic terminals. Regenerative intercellular calcium waves (ICWs) can travel over 100s of astrocytes, encompassing many neuronal synapses. These ICWs are documented in the control of synaptic activity. Glutamate is released in a regenerative manner, with subsequent cells that are involved in the calcium wave releasing additional glutamate (Ross, 2012).

$[Ca^{2+}]$ affect increased release probabilities at synaptic sites, likely due to triggering release of gliotransmitters. (Free Ca^{2+} waves are considered here, not intracellular astrocyte calcium waves in situ which also increase neuronal firings.)

Free regenerative Ca^{2+} waves, arising from astrocyte-neuron interactions, couple to the magnetic vector potential $\mathbf{A}$ produced by highly synchronous collective firings, e.g., during selective attention tasks, as measured by EEG.

4.4.1 Canonical Momentum $\mathbf{\Pi} = \mathbf{p} + q\mathbf{A}$

As derived in the Feynman (midpoint) representation of the path integral, the canonical momentum, $\mathbf{\Pi}$, describes the dynamics of a moving particle with momentum $\mathbf{p}$ in an electromagnetic field. In SI units,

$$\mathbf{\Pi} = \mathbf{p} + q\mathbf{A} \tag{15}$$

where $q = -2e$ for Ca^{2+}, e is the magnitude of the charge of an electron $= 1.6 \times 10^{-19}$ C (Coulomb), and $\mathbf{A}$ is the electromagnetic vector potential. (In Gaussian units $\mathbf{\Pi} = \mathbf{p} + q\mathbf{A}/c$, where c is the speed of light.) $\mathbf{A}$ represents three components of a 4-vector.

Classical-physics and quantum-physics calculations show that the momenta $\mathbf{p}$ of Ca^{2+} waves is comparable to $q\mathbf{A}$.

Recently work has included classical SMNI calculations of tripartite (neuron-astrocyte-neuron) interactions via Ca^{2+} Waves. Calculations are in progress using interactions between quantum tripartite interactions with classical SMNI models of highly synchronous neuronal firings.

4.4.2 Vector Potential of Wire

A columnar firing state is modeled as a wire/neuron with current $\mathbf{I}$ measured in A = Amperes = C/s,

$$\mathbf{A}(t) = \frac{\mu}{4\pi} \int \frac{dr}{r} \mathbf{I} \tag{16}$$

along a length z observed from a perpendicular distance r from a line of thickness r_0. If far-field retardation effects are neglected, this yields

$$\mathbf{A} = \frac{\mu}{4\pi} \mathbf{I} \log\left(\frac{r}{r_0}\right) \tag{17}$$

where μ is the magnetic permeability in vacuum $= 4\pi 10^{-7}$ H/m (Henry/meter). Note the insensitive log dependence on distance; this log factor is taken to be of order 1.

The contribution to $\mathbf{A}$ includes many minicolumnar lines of current from 100's to 1000's of macrocolumns, within a region not large enough to include many convolutions, but contributing to large synchronous bursts of EEG.

Electric $\mathbf{E}$ and magnetic $\mathbf{B}$ fields, derivatives of $\mathbf{A}$ with respect to r, do not possess this logarithmic insensitivity to distance, and therefore they do not linearly accumulate strength within and across macrocolumns.

Reasonable estimates of contributions from synchronous contributions to P300 measured on the scalp give tens of thousands of macrocolumns on the order of a 100 to 100's of cm^2, while electric fields generated from a minicolumn may fall by half within 5-10 mm, the range of several macrocolumns.

4.4.3 Effects of Vector Potential on Momenta

The momentum $\mathbf{p}$ for a Ca^{2+} ion with mass $m = 6.6 \times 10^{-26}$ kg, speed on the order of 50 μm/s to 100 μm/s, is on the order of 10^{-30} kg-m/s. Molar concentrations of Ca^{2+} waves, comprised of tens of thousands of free ions representing about 1% of a released set, most being buffered, are within a range of about 100 μm to as much as 250 μm, with a duration of more than 500 ms, and concentrations $[Ca^{2+}]$ ranging from 0.1-5 μM (μM $= 10^{-3}$ mol/m^3).

The magnitude of the current is taken from experimental data on dipole moments $\mathbf{Q} = |\mathbf{I}|z$ where $\hat{\mathbf{z}}$ is the direction of the current $\mathbf{I}$ with the dipole spread over z. $\mathbf{Q}$ ranges from 1 pA-m $= 10^{-12}$ A-m for a pyramidal neuron (Murakami and Okada, 2006), to 10^{-9} A-m for larger neocortical mass (Nunez and Srinivasan, 2006). These currents give rise to $q\mathbf{A} \approx 10^{-28}$ kg-m/s. The velocity of a Ca^{2+} wave can be ≈20-50 μm/s. In neocortex, a typical Ca^{2+} wave of 1000 ions, with total mass $m = 6.655 \times 10^{-23}$ kg times a speed of ≈20-50 μm/s, gives $\mathbf{p} \approx 10^{-27}$ kg-m/s.

Taking 10^4 synchronous firings in a macrocolumn, leads to a dipole moment $|\mathbf{Q}| = 10^{-8}$ A-m. Taking z to be $10^2\mu$m $= 10^{-4}$ m, a couple of neocortical layers, gives $|q\mathbf{A}| \approx 2 \times 10^{-19} \times 10^{-7} \times 10^{-8}/10^{-4} = 10^{-28}$ kg-m/s,

4.4.4 Reasonable Estimates

Estimates used here for $\mathbf{Q}$ come from experimental data, e.g., including shielding and material effects. When coherent activity among many macrocolumns associated with STM is considered, $|\mathbf{A}|$ may be orders of magnitude larger. Since Ca^{2+} waves influence synaptic activity, there is direct coherence between these waves and the activity of $\mathbf{A}$.

Classical physics calculates $q\mathbf{A}$ from macroscopic EEG to be on the order of 10^{-28} kg-m/s, while the momentum $\mathbf{p}$ of a Ca^{2+} ion is on the order of 10^{-30} kg-m/s. This numerical comparison illustrates the importance of the influence of $\mathbf{A}$ on $\mathbf{p}$ at classical scales.

The Extreme Science and Engineering Discovery Environment (XSEDE.org) project since February 2013, "Electroencephalographic field influence on calcium momentum waves," fit the SMNI model to EEG data, wherein ionic Ca^{2+} momentum-wave effects among neuron-astrocyte-neuron tripartite synapses modified parameterization of background SMNI parameters. Direct calculations in classical and quantum physics supported the concept that the vector magnetic potential of EEG from highly synchronous firings, e.g., as measured during selective attention, might directly interact with these momentum-waves, thereby creating feedback between these ionic/quantum and macroscopic scales (Ingber, 2012b,c, 2015, 2016b, 2017b; Ingber et al., 2014; Nunez et al., 2013).

4.5 Comparing Testing Data with Training Data

Using data from http://physionet.nlm.nih.gov/pn4/erpbci , SMNI was fit to highly synchronous waves (P300) during attentional tasks, for each of 12 subjects, it was possible to find 10 Training runs and 10 Testing runs (Citi et al., 2010; Goldberger et al., 2000).

Spline-Laplacian transformations on the EEG potential Φ are proportional to the SMNI M^G firing variables at each electrode site. The electric potential Φ is experimentally measured by EEG, not $\mathbf{A}$, but both are due to the same currents $\mathbf{I}$. Therefore, $\mathbf{A}$ is linearly proportional to Φ with a simple scaling factor included as a parameter in fits to data. Additional parameterization of background synaptic parameters, $B^G_{G'}$ and $B^{\ddagger E}_{E'}$, modify previous work.

The $\mathbf{A}$ model outperformed the no-$\mathbf{A}$ model, where the no-$\mathbf{A}$ model simply has used $\mathbf{A}$-non-dependent synaptic parameters. Cost functions with an $|\mathbf{A}|$ model were much worse than either the $\mathbf{A}$ model or the no-$\mathbf{A}$ model. Runs with different signs on the drift and on the absolute value of the drift also gave much higher cost functions than the $\mathbf{A}$ model.

5 Statistical Mechanics of Financial Markets (SMFM)

5.1 Quantum Money

Quantum computing is here, and in the near future it will be applied to financial products, e.g., blockchains. It not very far-fetched to assume that soon there will be financial derivatives developed on these products. Then, as is the case in classical real spaces with PATHTREE and PATHINT, qPATHTREE and qPATHINT are now poised to calculate financial derivatives in quantum complex spaces. This is beyond simply using quantum computation of financial derivatives, since the space of the dependent variables themselves may live in quantum worlds (Aaronson and Christiano, 2012; Accardi and Boukas, 2007; Baaquie et al., 2002; Jogenfors, 2016; Meyer, 2009; Piotrowski et al., 2005).

5.2 Previous Applications — PATHINT

Options V are generally described by a portfolio Π over an underlying asset S, where the real-world probability distribution of S often is critical to numerical details for trading. The asset is often hedged by trading the option V and a quantity Δ of the asset S.

$$d\Pi = \sigma \left(\frac{\partial V}{\partial S} - \Delta \right) dX + \left(\mu S \frac{\partial V}{\partial S} + \frac{1}{2} \sigma^2 S^2 \frac{\partial^2 V}{\partial S^2} + \frac{\partial V}{\partial t} - \mu \Delta S \right) dt$$

$$\Gamma = \frac{\partial^2 \Pi}{\partial S^2}, \Theta = \frac{\partial \Pi}{\partial t}, \Upsilon = \frac{\partial \Pi}{\partial \sigma}, \rho = \frac{\partial \Pi}{\partial r} \tag{18}$$

The portfolio Π to be hedged is often considered to be "risk-neutral," if Δ is chosen such that $\Delta = \frac{\partial V}{\partial S}$.

While quite a few closed-form solutions exist for European options (Black and Scholes, 1973), where there is not early exercise, for American options — among the most popular options — there is no general closed form, and numerical calculations must be performed (Hull, 2000). In the path-integral approach, first the probability "tree" for S is propagated forward in time until the expiration date T, branching out as extended S values develop.

Then, marching back in time, at each time-node various calculations can be performed, e.g., the Greeks above, inserting changes (often "shocks") in dividends, interest rates, changes in cheapest-to-deliver of a basket of bonds in the case of options on bond futures, etc (Ingber, 2000; Ingber and Wilson, 1999). This is similar to the use of the popular binomial-tree approach used by many trading firms.

Explicitly, at each node a calculation is performed, comparing the strike price X to the price S at that node, and a decision is made, e.g., whether to exercise the option at that node — determining the fair value of the option price V. To obtain the Greeks above, most derivatives of these Derivatives are calculated numerically by using values across branches and notes. The derivatives are often extended over more points to average of over derivative-induced noise.

5.2.1 Volatility of Volatility of American Options

An example of a two-dimensional options model processed by PATHINT developed the volatility of volatility of options on Eurodollars, using 2-factor model developed by the author:

$$dS = \mu \, S \, dt + \sigma \, F(S, S_0, S_\infty, x, y) \, dz_S$$

$$d\sigma = \nu \, dt + \epsilon \, dz_\sigma$$

$$F(S, S_0, S_\infty, x, y) = S, \; S < S_0$$

$$F(S, S_0, S_\infty, x, y) = S^x S_0^{1-x}, \; S_0 \leq S \leq S_\infty$$

$$F(S, S_0, S_\infty, x, y) = S^y S_0^{1-x} S_\infty^{x-y}, \; S > S_\infty \tag{19}$$

where S_0 and S_∞ are selected to lie outside the data region used to fit the other parameters, e.g., $S_0 = 1/2$ and $S_\infty = 20$ for fits to Eurodollar futures which historically have a very tight range relative to other markets.

5.2.2 SMFM Example of 2-Factor PATHINT

An example of a two-factor distribution evolved out to $T = 0.5$ year for $x = 0.7$ simply shows PATHINT at work in Fig. 4.

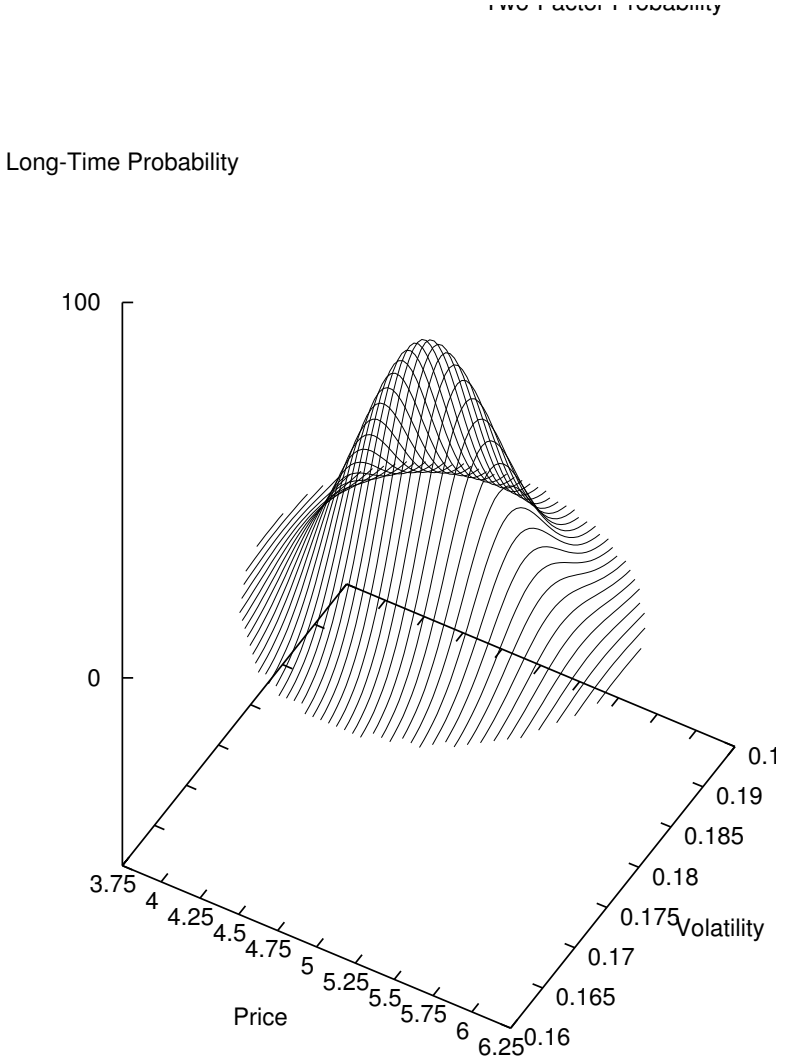

Figure 4 illustrates a two-factor distribution evolved out to $T = 0.5$ year for $x = 0.7$ (Ingber, 2000).

5.3 Application to Risk

As an aside, path integrals also have been applied to copula risk management. The approach to consider a basket of markets (a few, or thousands of markets) in their **dx** variables, each fit separately to real data, e.g., using a parameterized 2-tail exponential distribution. Then each market is transformed to a Gaussian distribution in their **dy** variables, and the collection of Gaussians now permits a multi-factor Gaussian to be developed from which meaningful considerations based on covariance can be based, e.g., for value at risk (VaR).

This gives a multivariate correlated process P in the dy variables, in terms of Lagrangians L and Action A,

$$P(dy) \equiv P(dy^1, ..., dy^N) = (2\pi dt)^{-\frac{N}{2}} g^{-\frac{1}{2}} \exp(-Ldt) \tag{20}$$

The Lagrangian L is

$$L = \frac{1}{2dt^2} \sum_{ij} dy^i g_{ij} dy^j \tag{21}$$

The effective action A_{eff}, presenting a "cost function" useful for sampling and optimization, is defined by

$$P(dy) = \exp(-A_{eff})$$

$$A_{eff} = Ldt + \frac{1}{2} \ln\, g + \frac{N}{2} \ln(2\pi dt) \tag{22}$$

5.3.1 Copula

The multivariate distribution in x-space is specified, including correlations, using

$$P(dx) = P(dy) \left| \frac{\partial\, dy^i}{\partial\, dx^j} \right| \tag{23}$$

where $\left| \frac{\partial dy^i}{\partial dx^j} \right|$ is the Jacobian matrix specifying this transformation. This yields

$$P(dx) = g^{-\frac{1}{2}} \exp\left(-\frac{1}{2} \sum_{ij} \left(dy^i_{dx}\right)^\dagger \left(g_{ij} - I_{ij}\right) \left(dy^j_{dx}\right) \right) \prod_i P_i(dx^i) \tag{24}$$

where $\left(dy_{dx}\right)$ is the column-vector of $\left(dy^1_{dx}, \ldots, dy^N_{dx}\right)$ expressed back in terms of their respective $\left(dx^1, ..., dx^N\right)$, $\left(dy_{dx}\right)^\dagger$ is the transpose row-vector, and $\left(I\right)$ is the identity matrix.

The Gaussian copula $C(dx)$ is defined by

$$C(dx) = g^{-\frac{1}{2}} \exp\left(-\frac{1}{2} \sum_{ij} \left(dy^i_{dx}\right)^\dagger \left(g_{ij} - I_{ij}\right) \left(dy^j_{dx}\right) \right) \tag{25}$$

Some additional work is performed to generate guaranteed stable numerical covariance matrices.

These calculations have been embedded as a middle layer in a program Trading in Risk Dimensions (TRD). An inner-shell of Canonical Momenta Indicators (CMI), momenta Π defined previously, is adaptively fit to incoming market data. A parameterized trading-rule outer-shell uses ASA to fit the trading system to historical data. An additional risk-management middle-shell is added to create a three-shell recursive optimization/sampling/fitting algorithm. Portfolio-level distributions of copula-transformed multivariate distributions are generated by Monte Carlo samplings. ASA is used to importance-sample weightings of these markets.

6 qPATHINT: Inclusion of Quantum Scales

6.1 PATHINT/qPATHINT Code

To numerically calculate the path integral, especially for serial changes in time — not approachable with standard Monte Carlo techniques — PATHINT was developed. the PATHINT C code of about 7500 lines of code was rewritten for the GCC C-compiler to use double complex variables instead of double variables. The code is written for arbitrary N dimensions. The outline of the code is

described here for classical or quantum systems, using generic coordinates q and x (Ingber, 2016a, 2017b,c):

This histogram procedure recognizes that the distribution (probabilities for classical systems, wave-functions for quantum systems) can be numerically approximated to a high degree of accuracy by sums of rectangles of height P_i and width Δq^i at points q^i.

6.1.1 Shocks

Many real-world systems propagate in the presence of continual "shocks":

6.1.2 SMNI

regenerative Ca^{2+} waves due to collisions
interactions with changing **A**

6.1.3 SMFM

future dividends
changes in interest rates
changes in asset distributions used in American options algorithms

6.1.4 PATHINT/qPATHINT Histograms

Considering a one-dimensional system in variable x, in the prepoint Ito discretization, the path-integral representation can be written in terms of the kernel G, for each of its intermediate integrals, as

$$P(x;t+\Delta t) = \int dx' [g^{1/2}(2\pi\Delta t)^{-1/2} \exp(-L\,\Delta t)] P(x';t) = \int dx' G(x,x';\Delta t) P(x';t)$$

$$P(x;t) = \sum_{i=1}^{N} \pi(x-x^i) P_i(t)$$

$$\pi(x-x^i) = 1\,,\ (x^i - \frac{1}{2}\Delta x^{i-1}) \le x \le (x^i + \frac{1}{2}\Delta x^i); 0\,,\ \text{otherwise} \tag{26}$$

This yields

$$P_i(t+\Delta t) = T_{ij}(\Delta t) P_j(t)$$

$$T_{ij}(\Delta t) = \frac{2}{\Delta x^{i-1} + \Delta x^i} \int_{x^i - \Delta x^{i-1}/2}^{x^i + \Delta x^i/2} dx \int_{x^j - \Delta x^{j-1}/2}^{x^j + \Delta x^j/2} dx' G(x,x';\Delta t) \tag{27}$$

T_{ij} is a banded matrix representing the Gaussian nature of the short-time probability centered about the (possibly time-dependent) drift.

Several projects have used this algorithm (Ingber and Nunez, 1995; Ingber et al., 1996; Ingber and Wilson, 1999; Wehner and Wolfer, 1983a,b, 1987). Special 2-dimensional codes were developed for specific projects in Statistical Mechanics of Combat (SMC), SMNI and SMFM (Ingber, 2000; Ingber et al., 1991; Ingber and Nunez, 1995).

6.1.5 Meshes For [q]PATHINT

Explicit dependence of L on time t also can be included without complications. Care must be used in developing the mesh Δq^i, which is strongly dependent on diagonal elements of the diffusion matrix, e.g.,

$$\Delta q^i \approx (\Delta t g^{|ii|})^{1/2} \tag{28}$$

This constrains the dependence of the covariance of each variable to be a (nonlinear) function of that variable to present a rectangular-ish underlying mesh. Since integration is inherently a smoothing process (Ingber, 1990), fitting the data with integrals over the short-time probability distribution, this permits the use of coarser meshes than the corresponding stochastic differential equation(s) (Wehner and Wolfer, 1983a).

For example, the coarser resolution is appropriate and typically required, for a numerical solution of the time-dependent path integral. By considering the contributions to the first and second moments, conditions on the time and variable meshes can be derived. Thus Δt can be measured by the diffusion divided by the square of the drift.

6.2 Lessons Learned From SMFM and SMNI

6.2.1 Broad-Banded Kernels Required

SMNI qPATHINT has emphasized the requirement of broad-banded kernels for oscillatory quantum states.

SMFM PATHTREE, and its derived qPATHTREE, is a different options code, based on path-integral error analyses, permitting a new very fast binary calculation, also applied to nonlinear time-dependent systems (Ingber et al., 2001).

However, in contrast to the present PATHINT/qPATHINT code that has been generalized to N dimensions, currently an SMFM [q]PATHTREE is only a binary tree with J = 1 and cannot be effectively applied to quantum oscillatory systems (Ingber, 2016a, 2017b,c).

6.2.2 Calculations At Each Node At Each Time Slice

SMFM (q)PATHINT proceeds as: Calculate at Each Node of Each Time Slice — Back in Time

SMNI (q)PATHINT proceeds as: Calculate at Each Node of Each Time Slice — Forward in Time

A lesson learned is that SMNI PATHINT can interact at each time slice with Ca^{2+}-wave qPATHINT.

6.2.3 SMFM qPATHINT With Serial Shocks

A University of California San Diego (UCSD) supercomputer resource is Comet: "Comet is a 2.0 Petaflop (PF) Dell integrated compute cluster, with next-generation Intel Haswell processors (with AVX2), interconnected with Mellanox FDR InfiniBand in a hybrid fat-tree topology. Full bisection bandwidth is available at rack level (72 nodes) and there is a 4:1 oversubscription cross-rack. Compute nodes feature 320 GB of SSD storage and 128GB of DRAM per node."

To appreciate requirements of kernel memory as a function of dimension, some N-dim qPATHINT runs for SMFM were considered in a pilot study, using a contrived N-factor model with the same 1-dimensional system cloned in all dimensions (each unit is a "double complex"):

D=1:imxall: 27 , jmxall: 7 , ijkcnt: 189
D=2:imxall: 729 , jmxall: 49 , ijkcnt: 35721

D=3:imxall: 19683 , jmxall: 343 , ijkcnt: 6751269
D=4:imxall: 531441 , jmxall: 2401 , ijkcnt: 1275989841
D=5:imxall: 14348907 , jmxall: 16807 , ijkcnt: 241162079949
D=6:imxall: 387420489 , jmxall: 117649 , ijkcnt: 45579633110361
D=7:imxall: 10460353203 , jmxall: 823543 , ijkcnt: 8614550657858229

The kernel size is $(\mathrm{I\,J})^{\mathrm{N}}$, where I = imxall, J = jmxall (= kernel band width), and kernel size = ijkcnt. This spatial mesh might change at each time slice.

A full set of ASA fits of classical SMNI to EEG data takes about 1000 hours of supercomputer CPUs; many such sets of runs are required to develop good models. Cost functions that include quantum processes will take even longer.

6.3 SMNI

Without random shocks, the wave function ψ_{e} representing the interaction of the EEG magnetic vector potential $\mathbf{A}$ with the momenta $\mathbf{p}$ of Ca^{2+} wave packets was derived in closed form from the Feynman (midpoint) representation of the path integral using path-integral techniques (Schulten, 1999)

$$\psi_{\mathrm{e}}(t) = \int d\mathbf{r}_0 \psi_0 \psi_F = \left[\frac{1 - i\hbar t/(m\Delta\mathbf{r}^2)}{1 + i\hbar t/(m\Delta\mathbf{r}^2)}\right]^{1/4} \left[\pi\Delta\mathbf{r}^2\{1 + [\hbar t/(m\Delta\mathbf{r}^2)]^2\}\right]^{-1/4}$$
$$\times \exp\left[-\frac{[\mathbf{r} - (\mathbf{\Pi}_0 + q\mathbf{A})t/m]^2}{2\Delta\mathbf{r}^2}\frac{1 - i\hbar t/(m\Delta\mathbf{r}^2)}{1 + [\hbar t/(m\Delta\mathbf{r}^2)]^2} + i\frac{\mathbf{\Pi}_0 \cdot \mathbf{r}}{\hbar} - i\frac{(\mathbf{\Pi}_0 + q\mathbf{A})^2 t}{2\hbar m}\right]$$

$$\psi_F(t) = \int \frac{d\mathbf{p}}{2\pi\hbar} \exp\left[\frac{i}{\hbar}\left(\mathbf{p}(\mathbf{r} - \mathbf{r}_0) - \frac{\mathbf{\Pi}^2 t}{(2m)}\right)\right] = \left[\frac{m}{2\pi i\hbar t}\right]^{1/2} \exp\left[\frac{im(\mathbf{r} - \mathbf{r}_0 - q\mathbf{A}t/m)^2}{2\hbar t} - \frac{i(q\mathbf{A})^2 t}{2m\hbar}\right]$$

$$\psi_0 = \psi(\mathbf{r}_0, t = 0) = \left(\frac{1}{\pi\Delta\mathbf{r}^2}\right)^{1/4} \exp\left(-\frac{\mathbf{r}_0^2}{2\Delta\mathbf{r}^2} + i\frac{\mathbf{\Pi}_0 \cdot \mathbf{r}_0}{\hbar}\right) \tag{29}$$

where ψ_0 is the initial Gaussian packet, ψ_F is the free-wave evolution operator, $\hbar$ is the Planck constant, q is the electronic charge of Ca^{2+} ions, m is the mass of a wave-packet of 1000 Ca^{2+} ions, $\Delta\mathbf{r}^2$ is the spatial variance of the wave-packet, the initial canonical momentum is $\mathbf{\Pi}_0 = \mathbf{p}_0 + q\mathbf{A}_0$, and the evolving canonical momentum is $\mathbf{\Pi} = \mathbf{p} + q\mathbf{A}$. Detailed calculations show that $\mathbf{p}$ of the Ca^{2+} wave packet and $q\mathbf{A}$ of the EEG field make about equal contributions to $\mathbf{\Pi}$.

Fits follow the time-dependent EEG data: SMNI synaptic parameters are affected by the model of Ca^{2+} waves. $\mathbf{A}$ derived from the EEG data affects the development of Ca^{2+} waves.

6.3.1 PATHINT SMNI + qPATHINT Ca^{2+} wave-packet

A proposed algorithm is to, at each node of each time slice, calculate quantum-scale Ca^{2+} wave-packet (2-way) interactions with macroscopic large-scale EEG/$\mathbf{A}$. This entails several algorithms:

PATHINT using the Classical SMNI Lagrangian
qPATHINT using the Quantum Ca^{2+} wave-packet Lagrangian

Sync in time during P300 attentional tasks.
Time/phase relations between classical and quantum systems may be important.

ASA-fit synchronized classical-quantum PATHINT-qPATHINT model to EEG data.
$\mathbf{A}$(EEG) is determined experimentally, and includes all synaptic background $B^G_{G'}$ effects.

Tripartite influence on synaptic $B^G_{G'}$ is measured by the ratio of packet's $< \mathbf{p}(t) >_{\psi * \psi}$ to $< \mathbf{p}_0(t_0) >_{\psi * \psi}$ at the onset of each attentional task. $\mathbf{A} = \sum_R \mathbf{A}_R \ln(R/R_0)$ from all R regions. Here $<>_{\psi * \psi}$ is taken over $\psi^*_{\rm e}\, \psi_{\rm e}$.

$$< \mathbf{p} >_{\psi * \psi} = m \frac{< \mathbf{r} >_{\psi * \psi}}{t - t_0} = \frac{q\mathbf{A} + \mathbf{\Pi}_0}{m^{1/2} |\Delta \mathbf{r}|} \left(\frac{(\hbar t)^2 + (m \Delta \mathbf{r}^2)^2}{\hbar t + m \Delta \mathbf{r}^2} \right)^{1/2} \tag{30}$$

Note that at $t = 0$, $< \mathbf{p} >_{\psi * \psi} = q\mathbf{A}$. $\mathbf{A}$ changes slower than $\mathbf{p}$, so static approximation of $\mathbf{A}$ used to derive $\psi_{\rm e}$ and $< \mathbf{p} >_{\psi * \psi}$ is reasonable to use within P300 EEG epochs, resetting $t = 0$ at the onset of each classical EEG measurement (1.953 ms apart), using the current $\mathbf{A}$. This permits tests of interactions across scales in a classical context.

6.3.2 Results Using $< \mathbf{p} >_{\psi * \psi}$

$< \mathbf{p} >_{\psi * \psi}$ was used in classical-physics SMNI fits to EEG data using ASA. Training with ASA used 100K generated states over 12 subjects with and without $\mathbf{A}$, followed by 1000 generated states with the simplex local code contained with ASA. Training and Testing runs on XSEDE.org for this project has taken an equivalent of several months of CPU on Comet described above. These calculations directly use $< \mathbf{p} >_{\psi * \psi}$ from Ca^{2+} wave packets, with one additional parameter across all EEG regions to weight the contribution to synaptic background $B^G_{G'}$. $\mathbf{A}$ is taken to be proportional to the currents measured by EEG, i.e., firings M^G. Otherwise, the "zero-fit-parameter" SMNI philosophy was enforced, wherein parameters are picked from experimentally determined values or within experimentally determined ranges (Ingber, 1984).

As with previous studies using this data, results sometimes give Testing cost functions less than the Training cost functions. This reflects on great differences in data, likely from great differences in subjects' contexts, e.g., possibly due to subjects' STM strategies only sometimes including effects calculated here. This confirms the need to further test these multiple-scale models with more EEG data, and with the PATHINT-qPATHINT coupled algorithm described above.

Table 1 gives recent results on such tests. Cost functions are the effective Action, A_{eff} above.

6.3.3 Quantum Zeno Effects

In the context of quantum mechanics, the wave function of the Ca^{2+} wave packet was calculated, and it was demonstrated that overlap with multiple collisions, due to their regenerative processes, during the observed long durations of hundreds of ms of typical Ca^{2+} waves support a Zeno or "bang-bang" effect which may promote long coherence times (Facchi et al., 2004; Facchi and Pascazio, 2008; Giacosa and Pagliara, 2014; Kozlowski et al., 2015; Muller et al., 2016; Patil et al., 2015; Wu et al., 2012; Zhang et al., 2014).

Of course, the Zeno/"bang-bang" effect may exist only in special contexts, since decoherence among particles is known to be very fast, e.g., faster than phase-damping of macroscopic classical particles colliding with quantum particles (Preskill, 2015).

Here, the constant collisions of Ca^{2+} ions as they enter and leave the Ca^{2+} wave packet due to the regenerative process that maintains the wave, may perpetuate at least part of the wave, permitting the Zeno/"bang-bang" effect. In any case, qPATHINT as used here provides an opportunity to explore the coherence stability of the wave due to serial shocks of this process.

Table 1: Column 1 is the subject number; the other columns are cost functions. Columns 2 and 3 are no-**A** model's Training (TR0) and Testing (TE0). Columns 4 and 5 are **A** model's Training (TR**A**) and Testing (TE**A**). Columns 6 and 7 are switched no-**A** model's Training (sTR0) and Testing (sTE0). Columns 8 and 9 are switched **A** model's Training (sTR**A**) and Testing (sTE**A**).

Sub	TR0	TE0	TR**A**	TE**A**	sTR0	sTE0	sTR**A**	sTE**A**
s01	85.75	121.23	84.76	121.47	120.48	86.59	119.23	87.06
s02	70.80	51.21	68.63	56.51	51.10	70.79	49.36	74.53
s03	61.37	79.81	59.83	78.79	79.20	61.50	75.22	79.17
s04	52.25	64.20	50.09	66.99	63.55	52.83	63.27	64.60
s05	67.28	72.04	66.53	72.78	71.38	67.83	69.60	68.13
s06	84.57	69.72	80.22	64.13	69.09	84.67	61.74	114.21
s07	68.66	78.65	68.28	86.13	78.48	68.73	75.57	69.58
s08	46.58	43.81	44.24	49.38	43.28	47.27	42.89	63.09
s09	47.22	24.88	46.90	25.77	24.68	47.49	24.32	49.94
s10	53.18	33.33	53.33	36.97	33.14	53.85	30.32	55.78
s11	43.98	51.10	43.29	52.76	50.95	44.47	50.25	45.85
s12	45.78	45.14	44.38	46.08	44.92	46.00	44.45	46.56

6.3.4 Survival of Wave Packet

In momentum space the wave packet, consider $\phi(\mathbf{p},t)$ being "kicked" from $\mathbf{p}$ to $\mathbf{p}+\delta\mathbf{p}$, and simply assume that random repeated kicks of $\delta\mathbf{p}$ result in $<\delta\mathbf{p}>\approx 0$, and each kick keeps the variance $\Delta(\mathbf{p}+\delta\mathbf{p})^2 \approx \Delta(\mathbf{p})^2$. Then, the overlap integral at the moment t of a typical kick between the new and old state is

$$
\begin{aligned}
&< \phi^*(\mathbf{p}+\delta\mathbf{p},t)|\phi(\mathbf{p},t) >= \exp\left(\frac{i\kappa+\rho}{\sigma}\right) \\
&\kappa = 8\delta\mathbf{p}\Delta\mathbf{p}^2\hbar m(q\mathbf{A}+\mathbf{p}_0)t - 4(\delta\mathbf{p}\Delta\mathbf{p}^2 t)^2 \\
&\rho = -(\delta\mathbf{p}\hbar m)^2 \\
&\sigma = 8(\Delta\mathbf{p}\hbar m)^2
\end{aligned}
\tag{31}
$$

where $\phi(\mathbf{p}+\delta\mathbf{p},t)$ is the normalized wave function in $\mathbf{p}+\delta\mathbf{p}$ momentum space. A crude estimate is obtained of the survival time $A(t)$ and survival probability $p(t)$ (Facchi and Pascazio, 2008),

$$
\begin{aligned}
A(t) &=< \phi^*(\mathbf{p}+\delta\mathbf{p},t)|\phi(\mathbf{p},t) > \\
p(t) &= |A(t)|^2
\end{aligned}
\tag{32}
$$

6.3.5 Calculation of Survival

These numbers yield:

$$
< \phi^*(\mathbf{p}+\delta\mathbf{p},t)|\phi(\mathbf{p},t) >= \exp\left(i(1.67\times10^{-1}t - 1.15\times10^{-2}t^2) - 1.25\times10^{-7}\right) \tag{33}
$$

Even many small repeated kicks do not appreciably affect the real part of ϕ, and these projections do not appreciably destroy the original wave packet, giving a survival probability per kick as $p(t) \approx \exp(-2.5\times10^{-7}) \approx 1 - 2.5\times10^{-7}$.

Both time-dependent phase terms in the exponent are sensitive to time scales on the order of 1/10 s, scales prominent in STM and in synchronous neural firings measured by EEG. This

suggests that **A** effects on Ca^{2+} wave functions may maximize their influence on STM at frequencies consistent with synchronous EEG during STM by some mechanisms not yet determined.

All these calculations support this model, in contrast to other models of quantum brain processes without such calculational support (Hagan et al., 2002; Hameroff and Penrose, 2013; McKemmish et al., 2009).

7 Applications

7.1 SMNI

7.1.1 Nano-Robotic Applications

To highlight the importance of research using nano-robots in the context of this project, there is the potential of carrying pharmaceutical products in nanosystems that could affect unbuffered Ca^{2+} waves in neocortex (Ingber, 2015). A Ca^{2+}-wave momentum-sensor could act like a piezoelectric device.

At the onset of a Ca^{2+} wave (on the order of 100's of ms), a change of momentum can be on the order of 10^{-30} kg-m/s for a typical Ca^{2+} ion. For a Ca^{2+} wave packet of 1000 ions with onset time of 1 ms, this gives a force on the order of 10^{-24} N (1 N $\equiv$ 1 Newton = 1 kg-m/s^2). The nanosystem would be attracted to this site, depositing chemicals/drugs that interact with the regenerative Ca^{2+}-wave process.

If the receptor area of the nanosystem were 1 nm^2 (the resolution of scanning confocal electron microscopy (SCEM)), this would require an extreme pressure sensitivity of 10^{-6} Pa (1 Pa = 1 pascal = 1 N/m^2).

The nanosystem could be switched on/off at a regional/columnar level by sensitivity to local electric/magnetic fields. Thus, piezoelectric nanosystems can affect background/noise efficacies at synaptic gaps via control of Ca^{2+} waves, affecting highly synchronous firings which carry many STM processes, which in turn affect the influence of of Ca^{2+} waves via the vector potential **A**, etc.

7.1.2 Free Will

In addition to the intrinsic interest of researching STM and multiple scales of neocortical interactions via EEG data, there is interest in researching possible quantum influences on highly synchronous neuronal firings relevant to STM to understand possible connections to consciousness and "Free Will" (FW) (Ingber, 2016a,b).

If neuroscience ever establishes experimental feedback from quantum-level processes of tripartite neuron-astrocyte-neuron synaptic interactions with large-scale synchronous neuronal firings, that are now recognized as being highly correlated with STM and states of attention, then FW may yet be established using the Conway-Kochen quantum no-clone "Free Will Theorem" (FWT) (Conway and Kochen, 2006, 2009).

Basically, this means that a Ca^{2+} quantum wave-packet may generate a state proven to have not previously existed; quantum states cannot be cloned.

7.2 SMFM

7.2.1 Quantum Money and Blockchains

Quantum computing is here, and in the near future it will be applied to financial products, e.g., blockchains. It is not very far-fetched to assume that soon there will be financial derivatives

developed on these products. Then, as is the case in classical real spaces with PATHTREE and PATHINT, qPATHTREE and qPATHINT are now poised to calculate financial derivatives in quantum complex spaces. This is beyond simply using quantum computation of financial derivatives, since the space of the dependent variables themselves may live in quantum worlds.

The marketplace will determine traded variables: For example, consider VIX, as a proxy for Volatility of Volatility of specific markets, is not the same as Volatility of Volatility for a single market, but exchanges list VIX.

7.2.2 Enhanced Security/Verification

As in SMNI, here too the core of the quantum no-clone "Free Will Theorem" (FWT) theorem can have important applications. Quantum currency cannot be cloned. Such currencies are exceptional candidates for very efficient blockchains, e.g., since each "coin" has a unique identity (Aaronson and Christiano, 2012; Bartkiewicz et al., 2016; Jogenfors, 2016; Meyer, 2009).

As in SMNI, here too there are issues about the decoherence time of such "coins".

8 Conclusion

A summary of a numerical path-integral methodology is presented, with emphasis on two different systems, in neuroscience and financial markets. Both SMNI and SMFM are generalized to include quantum variables. The SMFM method of calculation of financial options used at each time slice is adopted for SMNI. SMFM will require similar large kernel bands for oscillatory states.

In financial markets, the SMFM model has demonstrated it is faithful to experimental data, for financial options traded in real financial markets using the classical PATHINT algorithm. qPATHINT permits calculation of quantum options with serial shocks on quantum money, by evolving the quantum distribution of a quantum price variable, and calculating early exercise, marching back in time from the option maturity date.

In neuroscience, the SMNI model has demonstrated it is faithful to experimental data, for STM and EEG recordings under STM experimental paradigms. qPATHINT permits an inclusion of quantum scales in the multiple-scale SMNI model, by evolving Ca^{2+} wave-packets with momentum $\mathbf{p}$, including serial shocks, interacting with the magnetic vector potential $\mathbf{A}$ derived from EEG data, marching forward in time lock-step with experimental EEG data. This presents a time-dependent propagation of interacting quantum and classical scales.

Published pilot studies give a rationale for further developing this particular quantum path-integral algorithm based on folding kernels, as this can be used to study serial random shocks that occur in many real systems. Furthermore, this quantum version can be used for many quantum systems, which are becoming increasingly important as experimental data is increasing at a rapid pace for many quantum systems.

Acknowledgment

The author thanks the Extreme Science and Engineering Discovery Environment (XSEDE.org), for supercomputer grants since February 2013, starting with "Electroencephalographic field influence on calcium momentum waves", one under PHY130022 and two under TG-MCB140110. The current grant under TG-MCB140110, "Quantum path-integral qPATHTREE and qPATHINT algorithms", was started in 2017, and renewed through December 2018. XSEDE grants have spanned several projects described in

https://www.ingber.com/lir_computational_physics_group.html . The author also thanks Ronald Stesiak for a careful reading of a later draft of the manuscript.

$Id: https://www.ingber.com/path18_qpathint.pdf 1.21 2018/07/12 21:09:31$

References

S. Aaronson and P. Christiano, "Quantum money from hidden subspaces," MIT, Cambridge, MA, Tech. Rep. arXiv:1203.4740 [quant-ph], 2012.

L. Accardi and A. Boukas, "The quantum black-scholes equation," U di Roma Torvergata, Rome, Tech. Rep. arXiv:0706.1300 [q-fin.PR], 2007.

C. Agulhon, J. Petravicz, A. McMullen, E. Sweger, S. Minton, S. Taves, K. Casper, T. Fiacco, and K. McCarthy, "What is the role of astrocyte calcium in neurophysiology?" *Neuron*, vol. 59, pp. 932–946, 2008.

A. Araque and M. Navarrete, "Glial cells in neuronal network function," *Philosphical Transactions of The Royal Society B*, pp. 2375–2381, 2010.

J. Asher, "Brain's code for visual working memory deciphered in monkeys NIH-funded study," NIH, Bethesda, MD, Tech. Rep. NIH Press Release, 2012, http://www.nimh.nih.gov/news/science-news/2012/in-sync-brain-waves-hold-memory-of-objects-just-seen.shtml.

A. Atiya, A. Parlos, and L. Ingber, "A reinforcement learning method based on adaptive simulated annealing," in *Proceedings International Midwest Symposium on Circuits and Systems (MWCAS), December 2003*. Cairo, Egypt: IEEE CAS, 2003, https://www.ingber.com/asa03_reinforce.pdf.

B. Baaquie, C. Coriano, and M. Srikant, "Quantum mechanics, path integrals and option pricing: Reducing the complexity of finance," National U Singapore, Singapore, Tech. Rep. arXiv:cond-mat/0208191 [cond-mat.soft], 2002.

M. Banaclocha, I. Bookkon, and H. Banaclocha, "Long-term memory in brain magnetite," *Medical Hypotheses*, vol. 74, no. 2, pp. 254–257, 2010.

K. Bartkiewicz, A. Cernoch, G. Chimczak, K. Lemr, A. Miranowicz, and F. Nori, "Experimental quantum forgery of quantum optical money," Adam Mickiewicz University, Poznan, Poland, Tech. Rep. arXiv:1604.04453v1 [quant-ph], 2016.

S. Bellinger, "Modeling calcium wave oscillations in astrocytes," *Neurocomputing*, vol. 65, no. 66, pp. 843–850, 2005.

F. Black and M. Scholes, "The pricing of options and corporate liabilities," *The Journal of Political Economy*, vol. 81, no. 3, pp. 637–659, 1973.

F. Briggs, G. Mangun, and W. Usrey, "Attention enhances synaptic efficacy and the signal-to-noise ratio in neural circuits," *Nature*, vol. 000, pp. 1–5, 2013, http://dx.doi.org/10.1038/nature12276.

L. Citi, R. Poli, and C. Cinel, "Documenting, modelling and exploiting P300 amplitude changes due to variable target delays in Donchin's speller," *Journal of Neural Engineering*, vol. 7, no. 056006, pp. 1–21, 2010, http://dx.doi.org/10.1088/1741-2560/7/5/056006.

J. Conway and S. Kochen, "The free will theorem," Princeton U, Princeton, NJ, Tech. Rep. arXiv:quant-ph/0604079 [quant-ph], 2006.

J. Conway and S. Kochen, "The strong free will theorem," *Notices of the American Mathematical Society*, vol. 56, no. 2, pp. 226–232, 2009.

K. Ericsson and W. Chase, "Exceptional memory," *American Scientist*, vol. 70, pp. 607–615, 1982.

P. Facchi and S. Pascazio, "Quantum zeno dynamics: mathematical and physical aspects," *Journal of Physics A*, vol. 41, no. 493001, pp. 1–45, 2008.

P. Facchi, D. Lidar, and S. Pascazio, "Unification of dynamical decoupling and the quantum zeno effect," *Physical Review A*, vol. 69, no. 032314, pp. 1–6, 2004.

G. Giacosa and G. Pagliara, "Quantum zeno effect by general measurements," *Physical Review A*, vol. 052107, pp. 1–5, 2014.

A. Goldberger, L. Amaral, L. Glass, J. Hausdorff, P. Ivanov, R. Mark, J. Mietus, G. Moody, C.-K. Peng, and H. Stanley, "PhysioBank, PhysioToolkit, and PhysioNet: components of a new research resource for complex physiologic signals," *Circulation*, vol. 101, no. 23, pp. e215–e220, 2000, http://circ.ahajournals.org/cgi/content/full/101/23/e215.

S. Hagan, S. Hameroff, and J. Tuszynski, "Quantum computation in brain microtubules: Decoherence and biological feasibility," *Physical Review E*, vol. 65, no. 061901, pp. 1–11, 2002, http://link.aps.org/doi/10.1103/PhysRevE.65.061901.

S. Hameroff and R. Penrose, "Consciousness in the universe: A review of the 'Orch OR' theory," *Physics of Life Reviews*, vol. 403, pp. 1–40, 2013, http://dx.doi.org/10.1016/j.plrev.2013.08.002.

W. Hick, "On the rate of gains of information," *Quarterly Journal Experimental Psychology*, vol. 34, no. 4, pp. 1–33, 1952.

J. Hull, *Options, Futures, and Other Derivatives, 4th Edition.* Upper Saddle River, NJ: Prentice Hall, 2000.

L. Ingber, "Towards a unified brain theory," *Journal Social Biological Structures*, vol. 4, pp. 211–224, 1981, https://www.ingber.com/smni81_unified.pdf.

L. Ingber, "Statistical mechanics of neocortical interactions. i. basic formulation," *Physica D*, vol. 5, pp. 83–107, 1982, https://www.ingber.com/smni82_basic.pdf.

L. Ingber, "Statistical mechanics of neocortical interactions. dynamics of synaptic modification," *Physical Review A*, vol. 28, pp. 395–416, 1983, https://www.ingber.com/smni83_dynamics.pdf.

L. Ingber, "Statistical mechanics of neocortical interactions. derivation of short-term-memory capacity," *Physical Review A*, vol. 29, pp. 3346–3358, 1984, https://www.ingber.com/smni84_stm.pdf.

L. Ingber, "Statistical mechanics of neocortical interactions: Stability and duration of the 7+-2 rule of short-term-memory capacity," *Physical Review A*, vol. 31, pp. 1183–1186, 1985a, https://www.ingber.com/smni85_stm.pdf.

L. Ingber, "Towards clinical applications of statistical mechanics of neocortical interactions," *Innovations Technology Biology Medicine*, vol. 6, pp. 753–758, 1985b.

L. Ingber, "Statistical mechanics of neocortical interactions. EEG dispersion relations," *IEEE Transactions in Biomedical Engineering*, vol. 32, pp. 91–94, 1985c, https://www.ingber.com/smni85_eeg.pdf.

L. Ingber, "Very fast simulated re-annealing," *Mathematical Computer Modelling*, vol. 12, no. 8, pp. 967–973, 1989, https://www.ingber.com/asa89_vfsr.pdf.

L. Ingber, "Statistical mechanical aids to calculating term structure models," *Physical Review A*, vol. 42, no. 12, pp. 7057–7064, 1990, https://www.ingber.com/markets90_interest.pdf.

L. Ingber, "Statistical mechanics of neocortical interactions: A scaling paradigm applied to electroencephalography," *Physical Review A*, vol. 44, no. 6, pp. 4017–4060, 1991, https://www.ingber.com/smni91_eeg.pdf.

L. Ingber, "Generic mesoscopic neural networks based on statistical mechanics of neocortical interactions," *Physical Review A*, vol. 45, no. 4, pp. R2183–R2186, 1992, https://www.ingber.com/smni92_mnn.pdf.

L. Ingber, "Adaptive simulated annealing (ASA)," Caltech Alumni Association, Pasadena, CA, Tech. Rep. Global optimization C-code, 1993a, https://www.ingber.com/#ASA-CODE.

L. Ingber, "Statistical mechanics of combat and extensions," in *Toward a Science of Command, Control, and Communications*, C. Jones, Ed. Washington, D.C.: American Institute of Aeronautics and Astronautics, 1993b, pp. 117–149, ISBN 1-56347-068-3. https://www.ingber.com/combat93_c3sci.pdf.

L. Ingber, "Simulated annealing: Practice versus theory," *Mathematical Computer Modelling*, vol. 18, no. 11, pp. 29–57, 1993c, https://www.ingber.com/asa93_sapvt.pdf.

L. Ingber, "Statistical mechanics of neocortical interactions: Path-integral evolution of short-term memory," *Physical Review E*, vol. 49, no. 5B, pp. 4652–4664, 1994, https://www.ingber.com/smni94_stm.pdf.

L. Ingber, "Path-integral evolution of multivariate systems with moderate noise," *Physical Review E*, vol. 51, no. 2, pp. 1616–1619, 1995a, https://www.ingber.com/path95_nonl.pdf.

L. Ingber, "Statistical mechanics of multiple scales of neocortical interactions," in *Neocortical Dynamics and Human EEG Rhythms*, P. Nunez, Ed. New York, NY: Oxford University Press, 1995b, pp. 628–681, ISBN 0-19-505728-7. https://www.ingber.com/smni95_scales.pdf.

L. Ingber, "Statistical mechanics of neocortical interactions: Constraints on 40 hz models of short-term memory," *Physical Review E*, vol. 52, no. 4, pp. 4561–4563, 1995c, https://www.ingber.com/smni95_stm40hz.pdf.

L. Ingber, "Canonical momenta indicators of financial markets and neocortical EEG," in *Progress in Neural Information Processing*, S.-I. Amari, L. Xu, I. King, and K.-S. Leung, Eds. New York: Springer, 1996a, pp. 777–784, Invited paper to the 1996 International Conference on Neural Information Processing (ICONIP'96), Hong Kong, 24-27 September 1996. ISBN 981-3083-05-0. https://www.ingber.com/markets96_momenta.pdf.

L. Ingber, "Statistical mechanics of neocortical interactions: Multiple scales of EEG," in *Frontier Science in EEG: Continuous Waveform Analysis (Electroencephal. clin. Neurophysiol. Suppl.*

45), R. Dasheiff and D. Vincent, Eds. Amsterdam: Elsevier, 1996b, pp. 79–112, Invited talk to Frontier Science in EEG Symposium, New Orleans, 9 Oct 1993. ISBN 0-444-82429-4. https://www.ingber.com/smni96_eeg.pdf.

L. Ingber, "Adaptive simulated annealing (ASA): lessons learned," *Control and Cybernetics*, vol. 25, no. 1, pp. 33–54, 1996c, Invited paper to Control and Cybernetics on Simulated Annealing Applied to Combinatorial Optimization. https://www.ingber.com/asa96_lessons.pdf.

L. Ingber, "Statistical mechanics of neocortical interactions: Applications of canonical momenta indicators to electroencephalography," *Physical Review E*, vol. 55, no. 4, pp. 4578–4593, 1997a, https://www.ingber.com/smni97_cmi.pdf.

L. Ingber, *EEG Database*. Irvine, CA: UCI Machine Learning Repository, 1997b, http://archive.ics.uci.edu/ml/datasets/EEG+Database.

L. Ingber, "Data mining and knowledge discovery via statistical mechanics in nonlinear stochastic systems," *Mathematical Computer Modelling*, vol. 27, no. 3, pp. 9–31, 1998a, https://www.ingber.com/path98_datamining.pdf.

L. Ingber, "Statistical mechanics of neocortical interactions: Training and testing canonical momenta indicators of EEG," *Mathematical Computer Modelling*, vol. 27, no. 3, pp. 33–64, 1998b, https://www.ingber.com/smni98_cmi_test.pdf.

L. Ingber, "Statistical mechanics of neocortical interactions: Reaction time correlates of the g factor," *Psycholoquy*, vol. 10, no. 068, 1999, Invited commentary on The g Factor: The Science of Mental Ability by Arthur Jensen. https://www.ingber.com/smni99_g_factor.pdf.

L. Ingber, "High-resolution path-integral development of financial options," *Physica A*, vol. 283, no. 3-4, pp. 529–558, 2000, https://www.ingber.com/markets00_highres.pdf.

L. Ingber, "Trading in risk dimensions (TRD)," Lester Ingber Research, Ashland, OR, Tech. Rep. Report 2005:TRD, 2005, https://www.ingber.com/markets05_trd.pdf.

L. Ingber, "Statistical mechanics of neocortical interactions: Portfolio of physiological indicators," Lester Ingber Research, Ashland, OR, Tech. Rep. Report 2006:PPI, 2006a, https://www.ingber.com/smni06_ppi.pdf.

L. Ingber, "Ideas by statistical mechanics (ISM)," Lester Ingber Research, Ashland, OR, Tech. Rep. Report 2006:ISM, 2006b, https://www.ingber.com/smni06_ism.pdf.

L. Ingber, "Ideas by statistical mechanics (ISM)," *Journal Integrated Systems Design and Process Science*, vol. 11, no. 3, pp. 31–54, 2007, Special Issue: Biologically Inspired Computing.

L. Ingber, "AI and ideas by statistical mechanics (ISM)," in *Encyclopedia of Artificial Intelligence*, J. Rabunal, J. Dorado, and A. Pazos, Eds. New York: Information Science Reference, 2008, pp. 58–64, ISBN 978-1-59904-849-9.

L. Ingber, "Statistical mechanics of neocortical interactions: Portfolio of physiological indicators," *The Open Cybernetics Systemics Journal*, vol. 3, no. 14, pp. 13–26, 2009a, http://dx.doi.org/10.2174/1874110x00903010013.

L. Ingber, "Statistical mechanics of neocortical interactions: Nonlinear columnar electroencephalography," *NeuroQuantology Journal*, vol. 7, no. 4, pp. 500–529, 2009b, https://www.ingber.com/smni09_nonlin_column_eeg.pdf.

L. Ingber, "Computational algorithms derived from multiple scales of neocortical processing," in *Pointing at Boundaries: Integrating Computation and Cognition on Biological Grounds*, A. Pereira, Jr., E. Massad, and N. Bobbitt, Eds. New York: Springer, 2011, pp. 1–13, Invited Paper. https://www.ingber.com/smni11_cog_comp.pdf.

L. Ingber, "Adaptive simulated annealing," in *Stochastic global optimization and its applications with fuzzy adaptive simulated annealing*, H. Oliveira, Jr., A. Petraglia, L. Ingber, M. Machado, and M. Petraglia, Eds. New York: Springer, 2012a, pp. 33–61, Invited Paper. https://www.ingber.com/asa11_options.pdf.

L. Ingber, "Columnar EEG magnetic influences on molecular development of short-term memory," in *Short-Term Memory: New Research*, G. Kalivas and S. Petralia, Eds. Hauppauge, NY: Nova, 2012b, pp. 37–72, Invited Paper. https://www.ingber.com/smni11_stm_scales.pdf.

L. Ingber, "Influence of macrocolumnar EEG on ca waves," *Current Progress Journal*, vol. 1, no. 1, pp. 4–8, 2012c, https://www.ingber.com/smni12_vectpot.pdf.

L. Ingber, "Electroencephalographic (EEG) influence on Ca2+ waves: Lecture plates," Lester Ingber Research, Ashland, OR, Tech. Rep. Report 2013:LEFI, 2013, 2nd World Neuroscience Online Conference 18 June 2013. https://www.ingber.com/smni13_eeg_ca_lect.pptxandhttps://www.ingber.com/smni13_eeg_ca_lect.pdf.

L. Ingber, "Calculating consciousness correlates at multiple scales of neocortical interactions," in *Horizons in Neuroscience Research*, A. Costa and E. Villalba, Eds. Hauppauge, NY: Nova, 2015, pp. 153–186, ISBN: 978-1-63482-632-7. Invited paper. https://www.ingber.com/smni15_calc_conscious.pdf.

L. Ingber, "Path-integral quantum PATHTREE and PATHINT algorithms," *International Journal of Innovative Research in Information Security*, vol. 3, no. 5, pp. 1–15, 2016a, https://www.ingber.com/path16_quantum_path.pdf.

L. Ingber, "Statistical mechanics of neocortical interactions: Large-scale EEG influences on molecular processes," *Journal of Theoretical Biology*, vol. 395, pp. 144–152, 2016b, https://www.ingber.com/smni16_large-scale_molecular.pdf.

L. Ingber, "Quantum path-integral qPATHINT algorithm," *The Open Cybernetics Systemics Journal*, vol. 11, pp. 119–133, 2017a, https://www.ingber.com/path17_qpathint.pdf.

L. Ingber, "Evolution of regenerative ca-ion wave-packet in neuronal-firing fields: Quantum path-integral with serial shocks," *International Journal of Innovative Research in Information Security*, vol. 4, no. 2, pp. 14–22, 2017b, https://www.ingber.com/path17_quantum_pathint_shocks.pdf.

L. Ingber, "Options on quantum money: Quantum path-integral with serial shocks," *International Journal of Innovative Research in Information Security*, vol. 4, no. 2, pp. 7–13, 2017c, https://www.ingber.com/path17_quantum_options_shocks.pdf.

L. Ingber and R. Mondescu, "Automated internet trading based on optimized physics models of markets," in *Intelligent Internet-Based Information Processing Systems*, R. Howlett, N. Ichalkaranje, L. Jain, and G. Tonfoni, Eds. Singapore: World Scientific, 2003, pp. 305–356, Invited paper. https://www.ingber.com/markets03_automated.pdf.

L. Ingber and P. Nunez, "Statistical mechanics of neocortical interactions: High resolution path-integral calculation of short-term memory," *Physical Review E*, vol. 51, no. 5, pp. 5074–5083, 1995, https://www.ingber.com/smni95_stm.pdf.

L. Ingber, "Neocortical dynamics at multiple scales: EEG standing waves, statistical mechanics, and physical analogs," *Mathematical Biosciences*, vol. 229, pp. 160–173, 2010, https://www.ingber.com/smni10_multiple_scales.pdf.

L. Ingber and B. Rosen, "Genetic algorithms and very fast simulated reannealing: A comparison," *Mathematical Computer Modelling*, vol. 16, no. 11, pp. 87–100, 1992, https://www.ingber.com/asa92_saga.pdf.

L. Ingber and J. Wilson, "Volatility of volatility of financial markets," *Mathematical Computer Modelling*, vol. 29, no. 5, pp. 39–57, 1999, https://www.ingber.com/markets99_vol.pdf.

L. Ingber, "Statistical mechanics of financial markets: Exponential modifications to black-scholes," *Mathematical Computer Modelling*, vol. 31, no. 8/9, pp. 167–192, 2000, https://www.ingber.com/markets00_exp.pdf.

L. Ingber, H. Fujio, and M. Wehner, "Mathematical comparison of combat computer models to exercise data," *Mathematical Computer Modelling*, vol. 15, no. 1, pp. 65–90, 1991, https://www.ingber.com/combat91_data.pdf.

L. Ingber, R. Srinivasan, and P. Nunez, "Path-integral evolution of chaos embedded in noise: Duffing neocortical analog," *Mathematical Computer Modelling*, vol. 23, no. 3, pp. 43–53, 1996, https://www.ingber.com/path96_duffing.pdf.

L. Ingber, C. Chen, R. Mondescu, D. Muzzall, and M. Renedo, "Probability tree algorithm for general diffusion processes," *Physical Review E*, vol. 64, no. 5, pp. 056 702–056 707, 2001, https://www.ingber.com/path01_pathtree.pdf.

L. Ingber, M. Pappalepore, and R. Stesiak, "Electroencephalographic field influence on calcium momentum waves," *Journal of Theoretical Biology*, vol. 343, pp. 138–153, 2014, https://www.ingber.com/smni14_eeg_ca.pdf.

B. Innocenti, V. Parpura, and P. Haydon, "Imaging extracellular waves of glutamate during calcium signaling in cultured astrocytes," *Journal of Neuroscience*, vol. 20, no. 5, pp. 1800–1808, 2000.

A. Jensen, "Individual differences in the hick paradigm," in *Speed of Information-Processing and Intelligence*, P. Vernon, Ed. Norwood, NJ: Ablex, 1987, pp. 101–175.

J. Jogenfors, "Quantum bitcoin: An anonymous and distributed currency secured by the no-cloning theorem of quantum mechanics," Linkoping U, Linkoping, Sweden, Tech. Rep. arXiv:1604.01383 [quant-ph], 2016.

W. Kozlowski, S. Caballero-Benitez, and I. Mekhov, "Non-hermitian dynamics in the quantum zeno limit," U Oxford, Oxford, UK, Tech. Rep. arXiv:1510.04857 [quant-ph], 2015.

F. Langouche, D. Roekaerts, and E. Tirapegui, "Discretization problems of functional integrals in phase space," *Physical Review D*, vol. 20, pp. 419–432, 1979.

L. Ingber, *Functional Integration and Semiclassical Expansions.* Dordrecht, The Netherlands: Reidel, 1982.

L. McKemmish, J. Reimers, R. McKenzie, A. Mark, and N. Hush, "Penrose-hameroff orchestrated objective-reduction proposal for human consciousness is not biologically feasible," *Physical Review E*, vol. 80, no. 021912, pp. 1–6, 2009, http://link.aps.org/doi/10.1103/PhysRevE.80.021912.

K. Meyer, "Extending and simulating the quantum binomial options pricing model," U Manitoba, Winnipeg, Canada, Tech. Rep. Thesis, 2009, http://hdl.handle.net/1993/3154.

M. Muller, S. Gherardini, and F. Caruso, "Quantum zeno dynamics through stochastic protocols," U Florence, Florence, Italy, Tech. Rep. arXiv:1607.08871v1 [quant-ph], 2016.

S. Murakami and Y. Okada, "Contributions of principal neocortical neurons to magnetoencephalography and electroencephalography signals," *Journal of Physiology*, vol. 575, no. 3, pp. 925–936, 2006.

P. Nunez and R. Srinivasan, *Electric Fields of the Brain: The Neurophysics of EEG, 2nd Ed.* London: Oxford University Press, 2006.

P. Nunez, R. Srinivasan, and L. Ingber, "Theoretical and experimental electrophysiology in human neocortex: Multiscale correlates of conscious experience," in *Multiscale Analysis and Nonlinear Dynamics: From genes to the brain*, M. Pesenson, Ed. New York: Wiley, 2013, pp. 149–178, http://dx.doi.org/10.1002/9783527671632.ch06.

Y. Patil, S. Chakram, and M. Vengalattore, "Measurement-induced localization of an ultracold lattice gas," *Physical Review Letters*, vol. 115, no. 140402, pp. 1–5, 2015, http://link.aps.org/doi/10.1103/PhysRevLett.115.140402.

A. Pereira, Jr. and F. Furlan, "On the role of synchrony for neuron-astrocyte interactions and perceptual conscious processing," *Journal of Biological Physics*, vol. 35, no. 4, pp. 465–480, 2009.

E. Piotrowski, M. Schroeder, and A. Zambrzycka, "Quantum extension of european option pricing based on the ornstein-uhlenbeck process," *Physica A*, vol. 368, no. 1, pp. 176–182, 2005.

J. Preskill, "Quantum mechanics," Caltech, Pasadena, CA, Tech. Rep. Lecture Notes, 2015, http://www.theory.caltech.edu/people/preskill/ph219/.

R. Reyes and V. Parpura, "The trinity of Ca2+ sources for the exocytotic glutamate release from astrocytes," *Neurochemistry International*, vol. 55, no. 3, pp. 1–14, 2009.

W. Ross, "Understanding calcium waves and sparks in central neurons," *Nature Reviews Neuroscience*, vol. 13, pp. 157–168, 2012.

R. Salazar, N. Dotson, S. Bressler, and C. Gray, "Content-specific fronto-parietal synchronization during visual working memory," *Science*, vol. 338, no. 6110, pp. 1097–1100, 2012, http://dx.doi.org/10.1126/science.1224000.

E. Scemes and C. Giaume, "Astrocyte calcium waves: What they are and what they do," *Glia*, vol. 54, no. 7, pp. 716–725, 2006, http://dx.doi.org/10.1002/glia.20374.

L. Schulman, *Techniques and Applications of Path Integration.* New York: J. Wiley and Sons, 1981.

K. Schulten, "Quantum mechanics," U. Illinois, Urbana, IL, Tech. Rep. Lecture Notes, 1999, http://www.ks.uiuc.edu/Services/Class/PHYS480/.

A. Volterra, N. Liaudet, and I. Savtchouk, "Astrocyte Ca2+ signalling: an unexpected complexity," *Nature Reviews Neuroscience*, vol. 15, pp. 327–335, 2014.

M. Wehner and W. Wolfer, "Numerical evaluation of path-integral solutions to fokker-planck equations. I," *Physical Review A*, vol. 27, pp. 2663–2670, 1983a.

M. Wehner and W. Wolfer, "Numerical evaluation of path-integral solutions to fokker-planck equations. II. restricted stochastic processes," *Physical Review A*, vol. 28, pp. 3003–3011, 1983b.

M. Wehner and W. Wolfer, "Numerical evaluation of path integral solutions to fokker-planck equations. III. time and functionally dependent coefficients," *Physical Review A*, vol. 35, pp. 1795–1801, 1987.

S. Wu, L. Wang, and X. Yi, "Time-dependent decoherence-free subspace," *Journal of Physics A*, vol. 405305, pp. 1–11, 2012.

G. Zhang and H. Simon, "STM capacity for chinese words and idioms: Chunking and acoustical loop hypotheses," *Memory and Cognition*, vol. 13, pp. 193–201, 1985.

P. Zhang, Q. Ai, Y. Li, D. Xu, and C. Sun, "Dynamics of quantum zeno and anti-zeno effects in an open system," *Science China Physics, Mechanics and Astronomy*, vol. 57, no. 2, pp. 194–207, 2014, http://dx.doi.org/10.1007/s11433-013-5377-x.